# *Where Does the Density Localize in the Solid State? Divergent Behavior for Hybrids and DFT+U*



**Citation:** Zhao, Qing, and Heather J. Kulik. "Where Does the Density Localize in the Solid State? Divergent Behavior for Hybrids and DFT+U." Journal of Chemical Theory and Computation, vol. 14, no. 2, Feb. 2018, pp. 670–83. © 2018 American Chemical Society.

**As Published:** http://dx.doi.org/10.1021/ACS.JCTC.7B01061

**Publisher:** American Chemical Society (ACS)

**Persistent URL:** http://hdl.handle.net/1721.1/118959

**Version:** Final published version: final published article, as it appeared in a journal, conference proceedings, or other formally published context

JCTC Journal of Chemical Theory and Computation

Article

Cite This: J. Chem. Theory Comput. 2018, 14, 670−683

pubs.acs.org/JCTC

# Where Does the Density Localize in the Solid State? Divergent Behavior for Hybrids and DFT+U

Qing Zhao[†,‡] and Heather J. Kulik*[,†]

[†]Department of Chemical Engineering and [‡]Department of Mechanical Engineering, Massachusetts Institute of Technology, Cambridge, Massachusetts 02139, United States

Supporting Information

**ABSTRACT:** Approximate density functional theory (DFT) is widely used in chemistry and physics, despite delocalization errors that affect energetic and density properties. DFT+U (i.e., semilocal DFT augmented with a Hubbard U correction) and global hybrid functionals are two commonly employed practical methods to address delocalization error. Recent work demonstrated that in transition-metal complexes both methods localize density away from the metal and onto surrounding ligands, regardless of metal or ligand identity. In this work, we compare density localization trends with DFT+U and global hybrids on a diverse set of 34 transition-metal-containing solids with varying magnetic state, electron configuration and valence shell, and coordinating-atom orbital diffuseness (i.e., O, S, Se). We also study open-framework solids in which the metal is coordinated by molecular ligands, i.e., $MCO_3$, $M(OH)_2$, $M(NCNH)_2$, $K_3M(CN)_6$ (M = V−Ni). As in transition-metal complexes, incorporation of Hartree−Fock exchange consistently localizes density away from the metal, but DFT+U exhibits diverging behavior, localizing density (i) onto the metal in low-spin and late transition metals and (ii) away from the metal in other cases in agreement with hybrids. To isolate the effect of the crystal environment, we extract molecular analogues from open-framework transition-metal solids and observe consistent localization of the density away from the metal in all cases with both DFT+U and hybrid exchange. These observations highlight the limited applicability of trends established for functional tuning on transition-metal complexes even to equivalent coordination environments in the solid state.

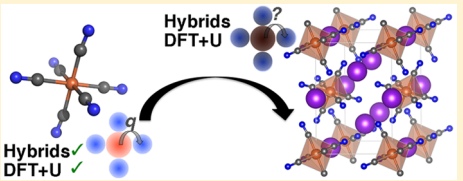


## 1. INTRODUCTION

Approximate density functional theory (DFT) is widely used to understand the electronic structure of transition-metal-containing molecules and materials. Nevertheless, presently available exchange-correlation (xc) approximations in DFT are plagued by both one- and many-electron self-interaction errors (SIE),[1−5] also referred to as delocalization error[6−8] (DE), which give rise to well-known problems in dissociation energies,[2,9−12] barrier heights,[13] band gaps,[14,15] and electron affinities.[16−18] Open shell transition-metal complexes and solids are particularly sensitive to imbalances in DE, which leads to strongly xc-dependent predictions of spin-state[19−24] or magnetic ordering[25−27] and thus electronic properties.

DE[6−8] has a quantitative energetic definition as the deviation from linearity with respect to exact piecewise linear behavior,[28] which also requires a derivative discontinuity,[29−32] with fractional addition or removal of an electron. The convex deviations[1,33] of pure xcs in approximate DFT (e.g., local density approximation, LDA, or generalized gradient approximation, GGA) from piecewise-linearity[34] are manifested in errors in numerous ground-state energetic and density properties. HF exchange conversely overlocalizes electrons and exhibits concave deviations[1,33] from piecewise linearity. These observations have motivated the incorporation of Hartree−Fock (HF) exchange through tuning[35−41] of global or range-separated hybrids[42−51] in which Janak's theorem[52] is invoked to identify[53] and eliminate deviations from piecewise linearity.

The limitation of this energetic definition is that as system size increases, the apparent deviation from linearity approaches zero,[54−57] making it a less suitable metric in solids. We recently demonstrated[58] that the DFT+U method,[59,60] widely employed for approximately treating SIE in semilocal DFT treatments of transition-metal chemistry,[61] can also recover piecewise linearity. We showed[58] that this piecewise linearity is not recovered at a calculated self-consistent,[19] linear-response[62,63] *U* but at one determined by the semilocal DFT deviation from linearity.[53]

Although DFT+U and hybrids represent suitable approaches for reduction of energetic DE in transition-metal chemistry, the effect on the density of energetic DE corrections remains unclear. It has been known for some time that functionals that provide good energetics (e.g., B3LYP[64−66]) yield poor densities in comparison to accurate references,[67] whereas others yield poor energetics and good densities.[68] Correct densities are a necessity for interpreting trends in chemical bonding[69] and associated observable quantities. This importance has been the recent focus of a surge in interest, especially in evaluating density errors of approximate DFT exchange correlation functionals in charged ions and small organic molecules.[70−73]

Received: October 19, 2017
Published: January 3, 2018

Less attention has been paid to how properties of *d*-[74,75] and *f*-[76,77] valence transition-metal complexes and solids are affected. Recently, we showed that global and range-separated hybrids as well as DFT+U universally localize the density away from the metal and onto surrounding ligand atoms in transition-metal complexes regardless of metal identity, spin state, ligand electronegativity, or ligand size.[22,74] These observations were consistent with studies that showed decreased bonding in 3*d* states (e.g., of CuCl[46] or in an iron octahedral complex[78]) and 4*f* states (e.g., lanthanide complexes[76]) with range-separated hybrids. In organic molecules, replacement of approximate DFT densities with ones derived from HF have been demonstrated to yield improved barrier heights[79,80] and dissociation energies,[6,81,82] enabling a separation of energetic- and density-driven delocalization errors.[6] Nevertheless, our recent work showed[74] that at the point of energetic DE elimination in molecules, residual density DE remained with respect to accurate correlated wave function theory reference densities.

The uniform localization of density away from the metal with all DE corrections was surprising given that the form of the DFT+U potential can either enhance or reduce *d* state occupations. Within the solid-state community, the Hubbard[83] and Anderson[84] model origins of DFT+U frequently invoke statements regarding electrons being localized onto a metal site, not away from it. It remains an open question whether functional tuning strategies with HF exchange and DFT+U have the same, convergent effect on solid-state properties as they do on transition-metal complexes. It is particularly useful to identify if hybrids and DFT+U perform comparably[74,85−87] due to the increased computational cost of evaluating long-range exchange in the solid state. Due to its low computational cost, DFT+U is often employed to open band gaps and recover the correct ground state in studies of transition-metal oxides, e.g., with Ce,[25,88,89] Ti,[90,91] Mn,[92−94] Fe,[92,93,95,96] Co,[92,93] and Ni[92,93] in various stoichiometries as well as to correct magnetic ordering in transition-metal-containing perovskites.[97] HF exchange, especially in computationally efficient short-range screened hybrids, can be used for similar purposes, e.g., in battery-relevant Ni- and Co-containing transition-metal oxides[98] as well as transition-metal monoxides[99] and di/trioxides[26,100−102] and perovskite materials,[27,103,104] sometimes with improvement over DFT+U results[99,105] for band gaps and structure or magnetic moments that motivate the higher computational cost of hybrids.

Despite the apparently similar effects of DFT+U and hybrids on energetics, few studies have compared how these methods alter the properties of the density in transition-metal-containing solids. In this work, we carry out a detailed comparison of the effect of HF exchange and DFT+U on 34 transition-metal-containing solids. Over this wide test set, we compare the effects of HF exchange and DFT+U on density in the solid state as we vary electron configuration, substituent size, and coordination environment in order to identify if they behave as similarly as they do in transition-metal complexes. Within a subset of open-framework solids, we make direct comparison to isolated molecules through rigid extraction of octahedral complexes from the solid-state environment. Such a study is revealing because it sheds light on whether functional tuning effects are transferable from small molecule chemistry, where experimental and accurate wave function theory references are abundant, to the solid state. The rest of this article is outlined as follows. In Section 2, we provide the computational details of the calculations employed in this work. In Section 3, we present trends in density localization for global hybrids and DFT+U in representative transition-metal oxides, sulfides, and selenides with early and late transition metals along with open-framework transition-metal solids and their molecular analogues. Finally, in Section 4, we provide our conclusions.

## 2. COMPUTATIONAL DETAILS

**Hybrid Calculations.** The effect of exact exchange was investigated by altering[22,74] the percentage of HF exchange in a modified form of the B3LYP[64−66] global hybrid functional from as low as 0% (i.e., pure BLYP GGA) to as high as 50% HF ($a_{HF}$ = 0.5) exchange in increments of 5%, unless otherwise noted

$$E_x^{\text{mod B3LYP}} = E_x^{\text{LDA}} + a_{\text{HF}}(E_x^{\text{HF}} - E_x^{\text{LDA}}) + 0.9(1 - a_{\text{HF}})(E_x^{\text{GGA}} - E_x^{\text{LDA}}) \quad (1)$$

while holding the GGA/LDA ratio fixed to the 9:1 value in standard (i.e., 20% exchange) B3LYP.[64−66] Hybrid DFT calculations on solids were performed using the periodic boundary condition (PBC) code CRYSTAL14[106] with a localized basis set (LBS). The default definition of B3LYP in CRYSTAL employs the VWN5 form for the LDA VWN[107] component of LYP[64] correlation. At least a double-ζ split-valence basis set was used for all atoms, with polarization added in some cases (3*d* Cr−Ni, and H, N, C, and K), and triple-ζ split-valence basis sets were used for Pt, with polarization added for Ir, as obtained from the CRYSTAL[106] Web site[108] (Supporting Information Table S1). Using larger triple-ζ split-valence basis sets yields comparable results on representative cases (Supporting Information Figure S1). All-electron calculations were carried out for all species except in the case of Mo, Ir, and Pt atoms where Hay-Wadt[109] effective core potentials were used, and only the semicore states of Mo (4*s*, 4*p*) or Ir and Pt (5*s*, 5*p*) were described explicitly along with the valence electrons.

The atomic positions and lattice parameters of all solids were fully optimized using the BFGS quasi-Newton algorithm[110−114] with default tolerances of $4.5 \times 10^{-4}$ hartree/bohr for the maximum gradient and $3.0 \times 10^{-4}$ hartree/bohr for the root mean squared gradient. Monkhorst−Pack *k*-point grids were used in all cases to sample the Brillouin zone: 12 × 12 × 12 for $MO_2$ transition-metal oxides, 6 × 6 × 6 for $TiX_2$ (X = S, Se), and 8 × 8 × 8 for the open-framework solids $M(NCNH)_2$, $M(OH)_2$, $MCO_3$, and $K_3M(CN)_6$ (M = V−Ni). In order to aid self-consistent field (SCF) convergence, an electronic temperature of 0.005 hartree was applied. All calculations were spin-polarized, and the spin value was assigned to obtain correct atomic spin for ferromagnetic or nonmagnetic states (Supporting Information Table S2).

Single point energy calculations of iron complexes extracted from open-framework solids with modified B3LYP were performed using the TeraChem[115,116] quantum chemistry package with a LBS. The default definition of B3LYP in TeraChem employs the VWN1-RPA form for the LDA VWN[107] component of LYP[64] correlation. Using the CRYSTAL default of LYP correlation (i.e., VWN5) yields unchanged trends with respect to the VWN1-RPA results obtained with TeraChem defaults (Supporting Information Figure S2). Fe was treated with the LANL2DZ effective core potential,[109,117] and the 6-31G* basis was used for the remaining atoms. Larger aug-cc-pVTZ basis sets yielded unchanged trends on representative cases (Supporting Information Figure S3). High-spin and low-spin iron multi-


DOI: 10.1021/acs.jctc.7b01061
J. Chem. Theory Comput. 2018, 14, 670−683

plicities were assigned as quintet and singlet for Fe(II) and sextet and doublet for Fe(III). All calculations were spin-unrestricted with virtual and open-shell orbitals level-shifted[118] by 1.0 and 0.1 eV, respectively, to aid SCF convergence to an unrestricted solution.

**DFT+U.** DFT+U[59−61,119] calculations for solids and complexes were performed using the PBC code Quantum-ESPRESSO,[120] which employs a plane-wave basis set (PWBS). The PBE[121] GGA was employed with ultrasoft pseudopotentials (USPPs)[122] obtained from the Quantum-ESPRESSO Web site.[123] A full list of USPPs used in this work is provided in Supporting Information Table S3. Plane-wave cutoffs were 35 Ry for the wave function and 350 Ry for the charge density. The atomic positions and lattice parameters of all transition-metal solids were fully optimized using the BFGS quasi-Newton algorithm[110−114] until the maximum residual forces on the atoms were smaller than $1 \times 10^{-3}$ Ry/bohr ($5 \times 10^{-4}$ hartree/bohr). For solid-state calculations, *k*-point sampling and smearing values were the same as in the CRYSTAL calculations. All transition-metal atoms were given an initial guess of 0.0 starting magnetization for nonmagnetic states and 1.0 for ferromagnetic states in spin-polarized calculations.

For transition-metal complexes, single point energy calculations were performed with the Martyna-Tuckerman scheme[124] to eliminate periodic image effects on molecules, and only the Γ point of the Brillouin zone is used in such cases. Cubic box dimensions, chosen to ensure good grid spacing for atomic charges, ranged from 15 to 20 Å depending on the size of the complex. A list of box dimensions for each complex is provided in Supporting Information Table S4. In complexes, all transition-metal atoms were given an initial guess of 0.05 starting magnetization for low-spin states and 1.0 starting magnetization for high-spin states, and total magnetizations were set as described for the hybrid calculations. The simplified DFT+U correction

$$E^{\mathrm{DFT+U}} = E^{\mathrm{DFT}} + \frac{1}{2}\sum_{I,\sigma}\sum_{nl} U^{I}_{nl}[\mathrm{Tr}(\mathbf{n}^{I,\sigma}_{nl}(\mathbf{1} - \mathbf{n}^{I,\sigma}_{nl}))] \tag{2}$$

was employed with *I* corresponding to transition-metal atom sites, *nl* is 3*d*-5*d*, and $\sigma$ is the spin index. Occupation matrices, **n**, are obtained from projections of extended states onto atomic states obtained during pseudopotential generation, as is standard practice:[61]

$$n^{I,\sigma}_{mm'} = \sum_{k,v} \langle \psi_{k,v} | \phi^{I}_{m'} \rangle \langle \phi^{I}_{m} | \psi_{k,v} \rangle \tag{3}$$

The Hubbard *U* values employed in this work ranged from 0 eV (i.e., pure PBE-GGA) to up to 10 eV in 1 eV increments, unless otherwise noted, following the common practice in studies of tuning *U* effects and typical ranges of *U* values employed.[61,125]

**Structure Preparation.** A total of 34 transition-metal solids, 8 transition-metal dioxides, 1 transition-metal disulfide, 1 transition-metal diselenide, and 24 open-framework solids, were studied in this work (representative structures shown in Figure 1 and Supporting Information Table S2). The experimental rutile-type tetragonal structures of transition-metal dioxides $MO_2$ (M = Ti, V, Nb, Mo, Ru, Rh, Ir, Pt), hexagonal structures of transition-metal disulfides/diselenides $TiX_2$ (X = S, Se), trigonal structures of $MCO_3$ (M = Mn−Ni) and $M(OH)_2$ (M = Mn, Co, Ni), orthorhombic structures of $M(NCNH)_2$ (M = Fe−Ni), and monoclinic structures of $K_3M(CN)_6$ (M = Mn−Co) were obtained from the Inorganic Crystal Structure Database (ICSD).[126] Analogous $MCO_3$ (M = V, Cr), $M(OH)_2$ (M = V, Cr, Fe), $M(NCNH)_2$ (M = V−Mn), and $K_3M(CN)_6$ (M = V, Cr, Ni) structures were built by replacing the metal atom in the closest available experimental structure (Supporting Information Table S5). All structures were optimized at each level of theory. The structures of extracted $Fe(II)(NCNH)_6$, $Fe(II)(CO_3)_6$, $Fe(II)(OH)_6$, and $Fe(III)(CN)_6$ complexes were generated using the supercell builder function in Avogadro[127] by building large cells from the corresponding fully optimized crystal structures at each tuning parameter and retaining only a single octahedral complex. Single point energies of complexes were obtained on the geometries from the solids (i.e., high-spin complex from the ferromagnetic solid, low-spin complex from the nonmagnetic solid).

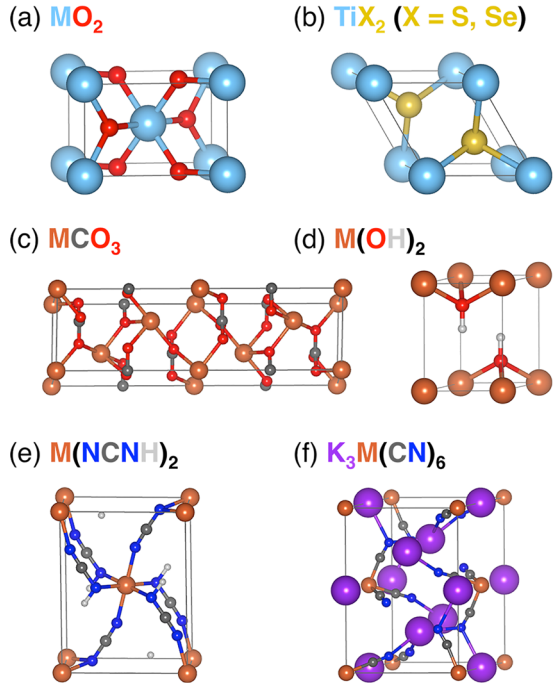


**Figure 1.** Structures of transition-metal compounds studied in this work. (a) transition-metal dioxides $MO_2$ (M = Ti, V, Nb, Mo, Ru, Rh, Ir, Pt) with a rutile-type tetragonal crystal structure, (b) transition-metal disulfides/diselenides $TiX_2$ (X = S, Se) with a hexagonal crystal structure, open-framework solids (c) $MCO_3$ and (d) $M(OH)_2$ with trigonal crystal structures, (e) $M(NCNH)_2$ with an orthorhombic crystal structure, and (f) $K_3M(CN)_6$ with a monoclinic crystal structure (M = V, Cr, Mn, Fe, Co, Ni).

**Partial Charges and Postprocessing.** For comparison of partial charges across two tuning procedures for both solids and complexes, we compute real-space Bader atomic charges[69,128] using the BADER program.[129] The grid resolutions were carefully selected to ensure convergence of partial charges and held constant across tuning methods for consistency (Supporting Information Table S6). Electron density cube files were obtained using the properties postprocessing code for CRYSTAL calculations, the pp.x postprocessing code for Quantum-ESPRESSO calculations, and the Multiwfn post-processing package[130] on Molden files obtained from TeraChem calculations.


DOI: 10.1021/acs.jctc.7b01061
J. Chem. Theory Comput. 2018, 14, 670−683

## 3. RESULTS AND DISCUSSION

**3a. Charge Localization in Representative Transition-Metal Oxides.** To determine the effect of DFT+U and HF exchange on densities in the solid state, we selected the frequently studied[90,91,131−134] and experimentally available rutile-type transition-metal (TM) dioxides ($MO_2$), in which a metal is surrounded by an octahedral environment of coordinating oxygen anions, producing a nonmagnetic (NM) ground state. From eight available structures, we study the effects of varying both *d*-electron configuration of the neutral metal ($d^2s^2$ in Ti to $d^9s^1$ in Pt) and the principal quantum number of the valence electrons (3*d*: Ti, V; 4*d*: Nb, Mo, Ru, Rh; and 5*d*: Ir, Pt). Both tuning strategies have small effects on equilibrium structures: optimizations with HF exchange decrease lattice parameters slightly (ca. 0.1 Å from GGA to 50% exchange), whereas DFT+U increases lattice parameters for early transition metals (i.e., Ti, V, and Nb, ca. 0.05−0.10 Å for GGA to $U$ = 10 eV) and has a smaller effect (ca. 0.02−3 Å) on mid or late transition metals (Supporting Information Table S7 and Figures S4−S5).

For the two functional tuning methods, there are slight differences in the GGA reference value: the $U$ = 0 eV in DFT+U corresponds to the pure PBE-GGA limit in a PWBS, and the 0% HF point is the pure BLYP-GGA limit in an LBS. Overall, the two GGA references used produce comparable Bader partial charges with small differences in absolute values for early transition metals (ca. 0.04−0.10 *e*) and slightly larger for late transition metals (ca. 0.10−0.29 *e*) (Figure 2). Trends of decreasing partial charge with *d*-filling (i.e., Ti to Pt) and increasing partial charge with increasing principal quantum number (i.e., V to Nb, Rh to Ir) are consistent across the two GGA references (Figure 2).

Regardless of metal identity, incorporation of HF exchange uniformly increases positive metal partial changes, signifying charge localization away from the metal and onto the surrounding oxygen anions. Increasing $U$ in DFT+U localizes partial charge away from the metal only for early transition metals (i.e., Ti, V, Nb) but onto the metal for midrow and late transition metals (i.e., Mo, Ru, Rh, Ir, Pt) (Figure 2). The increase in metal positive partial charge with incorporation of HF exchange is consistent with our observations on transition-metal complexes,[22,74] but DFT+U behavior with mid and late transition metals diverges from previous observations.[74]

Regardless of sign, approximately linear behavior of partial charges with tuning parameter is observed across the range of $U$ and $a_{HF}$ values studied (Figure 2). We thus use linear fits as approximations to the metal partial charge, $q_M$, sensitivities ($S$), i.e. the partial derivatives of $q_M$ with respect to the tuning parameters, $p$ (here, $U$ or $a_{HF}$):

$$S_p(q_M) = \frac{\Delta q_M}{\Delta p} \approx \frac{\partial q_M}{\partial p} \tag{4}$$

The units of $U$ are eV, and we use the unit notation "HFX" to represent the range from 0 to 100% HF exchange. The commonly proposed values of HF exchange in the literature range from around 0%[132,135] to at most 40−50%[98,103,136] (i.e., 0.4−0.5 HFX). In comparison, typical ranges of $U$ would be from 0 to around 6 eV.[98,135] Throughout the text, we commonly multiply $U$ sensitivities by 10 to compare to HF exchange sensitivities, roughly treating a change in HF exchange from 0 to 100% as equivalent to $U$ variations from 0 to 10 eV, consistent with our prior work.[74]

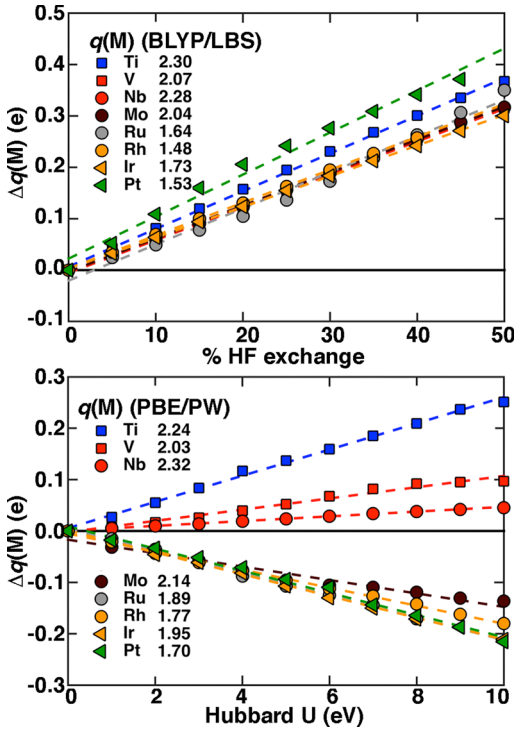


**Figure 2.** Dependence of shift of TM partial charge, $\Delta q$(M), in *e* with percentage of HF exchange (top) and $U$ (in eV, bottom) for nonmagnetic rutile-type $MO_2$ with M = Ti (blue squares), V (red squares), Nb (red circles), Mo (brown circles), Ru (gray circles), Rh (orange circles), Ir (orange triangles), and Pt (green triangles). The GGA partial charge is indicated in the inset, with all curves aligned to have zero $\Delta q$(M) values at the pure GGA value. The dashed lines indicate linear best fits through all data to quantify the partial charge sensitivities to HF exchange or $U$. Both HF exchange and Hubbard $U$ *y*-axes span the same 0.6 *e* range.

The changes in metal partial charge for rutile-type $MO_2$ correspond to an approximately 0.3 to 0.4 *e* loss from the metal with increasing HF exchange from GGA to 50% HF or a sensitivity of around 0.6−0.8 *e*/HFX (Figure 2). Comparing metal-dependent effects, the earliest, $TiO_2$, and latest, $PtO_2$, are most affected by HF exchange (ca. 0.4 *e* loss at 50% HF) with most midrow TMs reduced to around 0.3 *e* loss, excluding only $RuO_2$. As with dependence on electron configuration in the midrow, principal quantum number dependence is minimal, with comparable behavior for $VO_2$ and $NbO_2$ or $RhO_2$ and $IrO_2$. In contrast, for DFT+U with $U$ up to typically applied values of 6 eV, increasing *d* filling correlates with decreasing electron loss in early transition metals (i.e., Ti, V, Nb) from 0.15 *e* to 0.03 *e*, whereas midrow or late transition metals all gain around 0.10 *e* to 0.13 *e* from the oxygen atoms over the same range of $U$ values (Supporting Information Table S8). The divergent effect of DFT+U means that across the studied transition-metal dioxides, DFT+U demonstrates a larger range of charge sensitivities but smaller magnitude than HF exchange (Supporting Information Table S8).

We can compare charge sensitivities of these transition-metal dioxides with $M(OH_2)_6^{2+}$ (M = Ti, Fe, Ni) molecular complexes, which also have an oxygen-coordinating octahedral environment and are the most similar complexes in the literature.[74] HF exchange had a smaller effect on these molecules than on the solids, e.g. 0.23 *e*/HFX in $Ti(OH_2)_6^{2+}$ vs 0.8 *e*/HFX in $TiO_2$. In molecules, HF exchange sensitivity


DOI: 10.1021/acs.jctc.7b01061
J. Chem. Theory Comput. 2018, 14, 670−683

increased with increasing $d$ filling, whereas in the transition-metal dioxides there is no such trend. With DFT+U, the strong dependence of charge localization on $d$ filling in solids was conversely not observed in complexes.[74] For early transition metals, where DFT+U sensitivities are positive in both complexes and solids, the sensitivities are higher in the solids, e.g. 0.13 $e$/10 eV $U$ in $Ti(OH_2)_6^{2+}$ vs 0.25 $e$/10 eV $U$ in $TiO_2$.

Recalling the slight differences in geometry optimizations with incorporation of HF exchange or DFT+U, we confirmed that differing charge localization trends are not due to differences in each method's equilibrium lattice parameter. Comparing sensitivities of representative early $TiO_2$ and late $PtO_2$ cases at experimental instead of equilibrium lattice parameters reveals preserved sensitivities (see Supporting Information Figure S6).

Visualization of changes in the electron density at fixed lattice parameter with HF exchange and DFT+U confirms the direction of charge localization obtained from partial charge analysis (Figure 3). With HF exchange, we observe a spherically

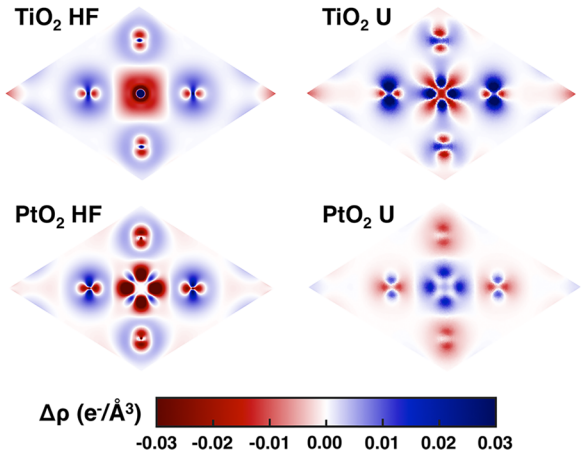


**Figure 3.** Electron density difference between 50% and 0% exchange for the rutile type $TiO_2$ (top left) and $PtO_2$ (bottom left) and between $U$ = 10 eV and $U$ = 0 eV for $TiO_2$ (top right) and $PtO_2$ (bottom right). Red and blue colors represent negative (electron density loss) and positive (electron density gain) electron density difference, respectively, as indicated by the inset color bar.

averaged loss of electron density from the area directly surrounding the metal (Ti or Pt) center and gain of electron density in the areas surrounding the O atoms. Consistent with observations in partial charge changes, DFT+U also shows density loss at the Ti metal in $TiO_2$, albeit with more $\delta$-orbital character to the density loss than the symmetric case for HF exchange. The density difference also confirms clear electron density loss from O atoms and gain at Pt for DFT+U only. Thus, divergent partial charge sensitivities for DFT+U and hybrids on late transition-metal oxides are evidence of a qualitative difference in the effect of the two methods that is not sensitive to real-space partitioning in the partial charge scheme or lattice parameter.

We can better understand the influence of the Hubbard $U$ on the density by reviewing the form of the Hubbard potential that is incorporated self-consistently:

$$V^U = \sum_{I,nl} \sum_{m} \frac{U^I_{nl}}{2}(1 - 2n^{I\sigma}_{nl,m})|\phi^I_{nl,m}\rangle\langle\phi^I_{nl,m}| \quad (5)$$

The potential acts to shift up (i.e., empty) occupied states with weak atomic occupation ($n$ < 1/2), and it fills occupied states with strong atomic occupation ($n$ > 1/2).[58,61,63] The potential has the opposite effect on unoccupied states, the efficiency of which was described in our recent work.[58] By reviewing occupation matrices and the potential employed in DFT+U (eqs 2, 3, and 5), we can thus rationalize the fundamentally different charge localization behaviors between early and late transition-metal dioxides. In the nonmagnetic states studied here, early transition metals have small fractional occupations that consistently empty with increasing $U$, whereas the least occupied states are still more than half-filled in late-row transition metals, leading to charge localization onto the metal through the DFT+U potential correction (Supporting Information Table S9).

Differences in changes in the density of states (DOS) with increasing HF exchange and DFT+U for early ($TiO_2$) and late ($PtO_2$) transition-metal dioxides can further clarify differences in the two functional tuning strategies (Figure 4). Experimentally, $TiO_2$ and $PtO_2$ have band gaps of 3.0 eV[137,138] and 0.2 eV,[139] respectively. HF exchange increases the band gap in $TiO_2$ from its GGA underestimate and introduces a band gap into metallic GGA $PtO_2$, whereas DFT+U weakly increases the $TiO_2$ band gap and maintains a metallic $PtO_2$ ground state (Figure 4 and Table 1). Hybrids[136,140] and DFT+U[92,141] are often used to open band gaps in GGA metals that are experimentally known insulators, but the optimal amount of exchange or $U$ is system-dependent. For DFT+U, the largest $U$ studied here (8 eV) increases the gap from the PBE/PWBS GGA reference but still underestimates the experimental value, and the gap in $PtO_2$ cannot be reproduced. In contrast, HF exchange tuning with high (i.e., 40%) exchange fractions can overestimate the band gaps (Table 1). Since the band gaps linearly increase with HF exchange, the optimal HF fraction can be interpolated to be 12−17% (for $TiO_2$ and $PtO_2$, respectively, Supporting Information Figure S7). In the case of $TiO_2$, this value can be compared to using the often-recommended inverse of the static dielectric ($1/\varepsilon$ = 0.18[143]) constant of the material,[104,142] which would overestimate the experimental band gap if used directly (Table 1).

Examination of projected density of states (PDOS) features in the valence band (VB) and conduction band (CB) edges also provide orbital-specific information about changes in states that give rise to the observed partial charge sensitivities. Integrating the individual and total $d$-orbital PDOS for Ti in $TiO_2$ and Pt in $PtO_2$ in the VB as HF exchange or $U$ is varied reveals comparable trends to Bader charge analysis and visualization of spatial density differences (Supporting Information Table S10). HF exchange (50%) in $TiO_2$ reduces equally occupied $d$-orbitals with GGA by around 0.2−0.25 $e$/HFX each and sharpens a sub-VB-edge $yz$ peak. Consistent with observations on the density differences, DFT+U instead selectively decreases the $x^2-y^2$ orbital occupancy by 0.20 $e$/10 eV $U$ from its GGA value, leaves the $xy$ occupancy unchanged, and decreases the occupancy in the remaining orbitals by a more modest amount (Supporting Information Table S10). In $PtO_2$, HF exchange reduces nearly equally the occupied $d$-orbitals by 0.9 $e$/HFX, which is in excess of the partial charge sensitivity likely due to increasing $s$ occupancy. The previously observed increase in DFT+U partial charges with $PtO_2$ is reflected in modest increases across all orbitals, except $z^2$, by an amount less than the partial charge sensitivity due to simultaneously increasing $s$ occupancy. Other differences evident from the full PDOS


DOI: 10.1021/acs.jctc.7b01061
J. Chem. Theory Comput. 2018, 14, 670−683

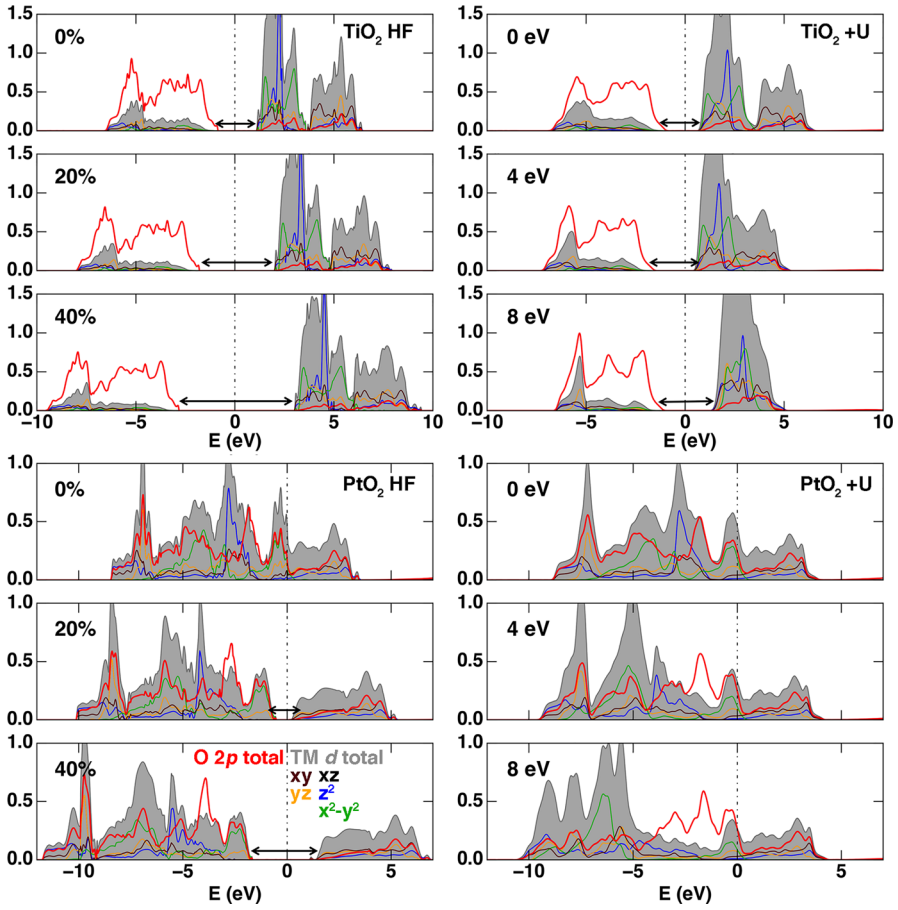


**Figure 4.** Projected density of states (PDOS) of (i) nonmagnetic $TiO_2$ (top) or $PtO_2$ (bottom) $d$ total (gray shaded region) and components: $d_{xy}$ (maroon line), $d_{yz}$ (orange line), $d_{xz}$ (black line), $d_{z^2}$ (blue line), $d_{x^2-y^2}$ (green line), and (ii) O 2$p$ total (red line). Plots on the left correspond to variation of HF exchange, whereas DFT+U variation is shown at the right with values indicated in insets. Arrows indicate the band gap opening with increasing HF exchange percentage and $U$ values around the Fermi level (vertical dashed line). The range in eV of the PDOS is smaller for $PtO_2$ than for $TiO_2$.

**Table 1. Band Gaps of $TiO_2$ and $PtO_2$ with HF Exchange and DFT+U**

| | $TiO_2$ | $PtO_2$ |
|---|---|---|
| BLYP/LBS | 1.91 eV | 0.0 eV |
| 40% exchange | 5.81 eV | 2.72 eV |
| $1/\varepsilon$ exchange | 3.70 eV | -- |
| PBE/PWBS | 1.39 eV | 0.0 eV |
| DFT+U (8 eV) | 2.19 eV | 0.0 eV |
| expt | 3.0 eV[137,138] | 0.2 eV[139] |

include both narrowing of the CB in $TiO_2$ and a delocalization of the $z^2$ $d$ state in the VB of $PtO_2$ with DFT+U that do not occur with HF exchange.

**3b. Ligand Diffuseness.** A commonly invoked explanation of the effect of SIE in correlated solids is that typically well-localized 3$d$ electrons are more affected by SIE than the more extended bonding states formed by other atoms. It would follow from this argument that SIE should cause the electron density to delocalize from 3$d$ states to neighboring atoms. Within molecules, we have recently demonstrated[74] that 3$d$ states are actually relatively delocalized compared to ligand atomic orbitals in 3$d$-2$p$ transition-metal coordination environments (e.g., 3$d$: 1.9 Å radius vs 2$p$: 1.7 Å radius for an 0.001 $e$ isosurface).[74] We also showed[74] that increasing the diffuseness of molecular ligand states (e.g., to 4$p$ or larger) with respect to the 3$d$ metal-centered orbitals so that 3$d$ states are, relatively speaking, well-localized instead increases the degree of delocalization from the metal to the ligand. The differences in transition-metal dioxides (Section 3a) motivate revisiting the possibility that coordination environment diffuseness could lead to different behavior with functional tuning in solids.

We select rutile $TiO_2$ as a representative system where both HF exchange and DFT+U localize density away from the metal and onto the surrounding oxygen atoms and examine if replacing oxygen changes charge localization patterns. To study larger-than-3$d$ coordinating atom valence electrons[74] (i.e., 3$p$ and 4$p$), we calculate properties of $TiS_2$ and $TiSe_2$ in their experimental hexagonal phases (Figure 5, inset). The structural difference between rutile and hexagonal octahedral environments is a slightly larger asymmetry in the rutile structure compared to more symmetric hexagonal structures (Supporting Information Figure S4 and Figure 5). The partial charges for the two GGA references (i.e., BLYP/LBS or PBE/PWBS) are relatively close and follow the same trend with increasingly heavy elements (Figure 5). With increasing valence orbital diffuseness, the Ti partial charge decreases (i.e., becomes more neutral), consistent with both changes in electronegativity, $\chi$ (Pauling scale − O: 3.4 > S: 2.6 = Se: 2.6), and previously studied transition-metal complexes[74] (Figure 5).

Importantly, all partial charge sensitivities are positive for the three solids, indicating density localization away from the metal,


DOI: 10.1021/acs.jctc.7b01061
J. Chem. Theory Comput. 2018, 14, 670−683

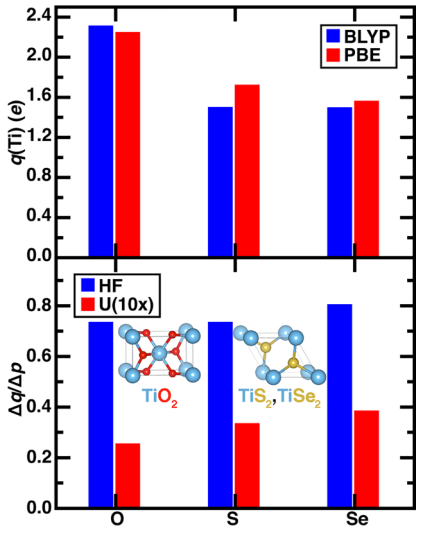


**Figure 5.** (top) Ti GGA reference partial charges in $e$ for $U$ (PBE/PWBS, red bars) or HF exchange (BLYP/LBS, blue bars) without any tuning and (bottom) Ti partial charge sensitivity to changes in $U$ ($e$/10 eV $U$, as indicated in legend, red bars) and HF exchange ($e$/HFX, blue bars). Crystal structures for rutile-type tetragonal $TiO_2$ and hexagonal $TiX_2$ (X = S, Se) are shown in the inset.

regardless of the functional tuning approach (Figure 5). For increasingly diffuse connecting atom valence orbitals (i.e., O to S to Se), the positive sensitivities increase in magnitude for all tuning methods, with monotonic increases for DFT+U and less elemental dependence for HF exchange (Figure 5). Thus, unlike early-to-late transition-metal trends in the oxides (Section 3a), metal-to-ligand density localization trends are consistent between DFT+U and hybrids when substituting with increasingly heavy coordinating atoms.

**3c. Charge Localization in Representative Open-Framework Solids.** The divergent behavior of DFT+U in transition-metal dioxides from that previously observed in molecules motivates the study of solids that resemble transition-metal complexes and from which isolated octahedral transition-metal complexes can be extracted (Section 3d). We thus constructed a test set of 24 open-framework solids, in which first-row transition metals (M = V−Ni) are coordinated by ligand-like moieties of two atoms or more. The four crystal structures have varying oxidation states: M(III) in $K_3M(CN)_6$ and M(II) in $M(NCNH)_2$ or oxygen-coordinating $M(OH)_2$ and $MCO_3$ (see structures in Figure 1 and details in Section 2). Across these structures, the ligand field strength should nominally vary as $CN^- > NCNH^- > OH^- \sim OCOO^{2-}$. We study all open-framework solids in both their nonmagnetic (NM) and ferromagnetic (FM) states to identify the effect of HF exchange or DFT+U on both density-localization trend variations between magnetic states. As in transition-metal dioxides, lattice parameters change slightly from GGA reference values with functional tuning: decreasing around 0.1 Å with HF exchange and either increasing or decreasing by around 0.05 Å in a system-dependent fashion with DFT+U (Supporting Information Table S11).

$M(OH)_2$ most strongly resembles the transition-metal dioxides (Section 3a): experimentally, it is a trigonal structure with an octahedral environment of oxygen atoms from hydroxyl groups coordinating the metal. As with the transition-metal dioxides, increasing HF exchange consistently increases the metal partial charges in both NM and FM states, regardless of electron configuration of the metal (Figure 6). In comparison

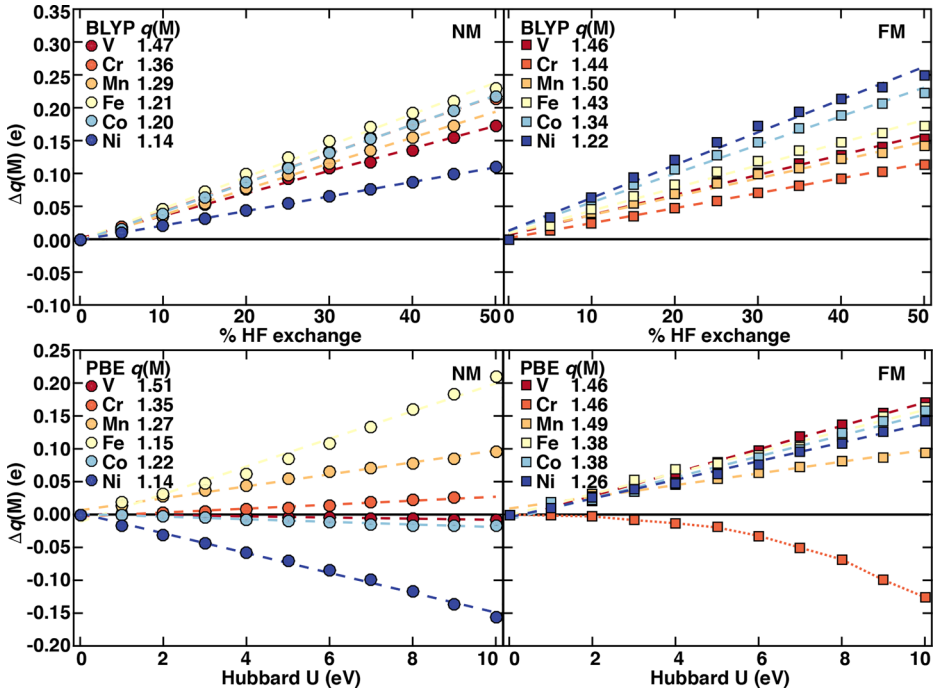


**Figure 6.** Dependence of shift of transition-metal partial charge, $\Delta q$(M), in $e$, for NM states (left, circle symbols) and FM states (right, square symbols) of $M(OH)_2$ with M = V (maroon), Cr (red), Mn (orange), Fe (yellow), Co (light blue), and Ni (dark blue). The GGA partial charge is indicated in the inset to allow alignment of the $\Delta q$(M) values to zero at 0% HF and $U$ = 0 eV. The dashed lines indicate linear best-fit lines to quantify the partial charge sensitivities, and the dotted lines indicate a nonlinear fit. All HF exchange and $U$ plots span the same 0.45 $e$ partial charge shift range.



DOI: 10.1021/acs.jctc.7b01061
J. Chem. Theory Comput. 2018, 14, 670−683

Table 2. Comparison of Partial Charges at Different Levels of Theory for Representative Solids

| | $Ni(OH)_2$ | | | $Cr(OH)_2$ | | |
|---|---|---|---|---|---|---|
| method | NM | FM | $q$(FM-NM) | NM | FM | $q$(FM-NM) |
| GGA (PBE/PWBS) | 1.14 | 1.26 | 0.12 | 1.35 | 1.46 | 0.11 |
| DFT+U (10 eV) | 0.98 | 1.41 | 0.43 | 1.37 | 1.33 | −0.04 |
| 50% HF exchange | 1.24 | 1.47 | 0.23 | 1.57 | 1.56 | −0.01 |

to sensitivities for the transition-metal dioxides, $M(OH)_2$ sensitivities are reduced in both magnetic states (Figure 6 and Supporting Information Table S12). These $M(OH)_2$ sensitivities are also more similar to those in transition-metal complexes.[74] Examining $d$-configuration dependence, midrow TMs have the highest NM sensitivities, whereas sensitivity appears to increase nearly monotonically with $d$ filling in the FM states. Although positive sensitivities are also highest for DFT+U in midrow Fe for the NM state, negative or near-zero sensitivities are observed for 3 metals (V, Co, Ni) in the NM state and one in the FM state (Cr). This range of charge sensitivities is comparable to that observed in the transition-metal dioxides, and thus additional ligand structure does not eliminate negative partial charge sensitivities with DFT+U. Examining possible underlying correlations across the first row TMs in $M(OH)_2$ reveals no relationship between partial charge magnitudes and sensitivities, unlike previous work on a narrower range of complexes;[22] but sensitivities generally increase with $d$ filling, and the magnitudes of the sensitivities are somewhat correlated between DFT+U and HF exchange even when signs differ (Supporting Information Figures S8−S10).

Reviewing sensitivities in the three other open-framework structures (i.e., $MCO_3$, $M(NCNH)_2$, and $K_3M(CN)_6$) reveals ligand-dependent effects. Comparable field strength environments (i.e., $MCO_3$ vs $M(OH)_2$) have similar overall sensitivities, and DFT+U sensitivities are again both positive and negative (Supporting Information Table S12). Trends of highest sensitivities for late TMs in FM states and highest sensitivities for midrow TMs in NM states are consistent for $MCO_3$ and $M(OH)_2$ solids (Supporting Information Table S12). Thus, consistent with prior observations in molecules,[22,24] the overall crystal structure has limited effect on charge localization as long as the direct ligand atom, and thus field strength, remains the same.

For intermediate-field $NCNH^-$ in $M(NCNH)_2$, $S_{HF}(q)$ values are comparable to the prior two weak-field cases in the NM state, and FM $S_{HF}(q)$ values are reduced slightly (Supporting Information Table S12). For DFT+U, negative sensitivities are slightly reduced in magnitude or even change sign (e.g., for FM $Cr(NCNH)_2$), likely due to greater delocalization of metal density into the more covalent bond that produces lower occupations (Supporting Information Table S12). Sensitivities of the closest available literature high-spin transition-metal complexes with intermediate-field $NH_3$ ligands[74] are comparable to HF and DFT+U sensitivities in FM states of $M(NCNH)_2$.

For the strongest field case considered, $K_3M(CN)_6$, the metal is also in a formal M(III) oxidation state. In this case, NM $S_{HF}(q)$ are reduced with respect to the M(II) compounds, again with highest values for midrow TMs, whereas values for FM $S_{HF}(q)$ are comparable to M(II) cases and also consistently increase with $d$ filling (Supporting Information Table S12). Large, uniformly negative sensitivities are observed for DFT+U in both states, highlighting the expected overriding dependence on formal oxidation state rather than on the ligand field strength or magnetic state (Supporting Information Table S12). Comparing ligand-field-strength trends in partial charge sensitivity with both HF and $U$, subtle ligand-derived trends ($CN^- < NCNH^- \leq OH^- = OCOO^{2-}$) approximately hold in open-framework solids, in analogy to the trends in transition-metal complexes ($CO < H_2O \leq NH_3$).[74]

Having confirmed that DFT+U and HF exchange exhibit diverging behavior across a range of TM solids that was not previously observed in TM complexes, we can quantify how functional tuning will alter the electronic properties of NM and FM states in representative $M(OH)_2$ solids. Relatively comparable Ni GGA partial charges in NM and FM states differ substantially with DFT+U due to negative NM and positive FM charge sensitivities but remain similar with HF exchange (Table 2). In contrast, $Cr(OH)_2$ charges tuned with HF exchange or DFT+U become even more comparable than predicted with GGA between states but for different reasons: (i) with HF exchange, charges in both magnetic states are tuned in the same direction but with different rates and (ii) for DFT+U charge sensitivities have opposite signs in the two magnetic states (Table 2).

Summarizing overall charge sensitivity trends, NM and FM states exhibit differing sensitivities due to differences in delocalization, as was previously observed in isolated molecules. These trends are made more complex by the fact that DFT+U exhibits both positive and negative partial charge sensitivities, whereas HF exchange uniformly localizes density away from metal sites. We also note that GGA functionals have a well-known[20−22] preference for low-spin states over high-spin states due to greater delocalization[61,74] afforded in low-spin states, whereas inclusion of HF exchange[20−22] or DFT+U[19,86,125,144] often reverses this preference. As in the case of diverging behavior of density localization, we also observe unexpected cases (e.g., $Fe(OH)_2$ for DFT+U and $FeCO_3$ for hybrids) where nonmagnetic cases are instead stabilized (Supporting Information Text S1, Tables S13−S15, and Figure S11). This unexpected behavior diverges from previous studies on complexes, motivating a more detailed comparison of density and magnetic ordering trends between open-framework solids and their inorganic complex analogues.

**3d. Extracted Transition-Metal Complex Analogues from Solids.** To isolate the role of the crystalline environment in functional sensitivities of energetic and density properties, we constructed transition-metal complexes by extracting the octahedral coordination environment from representative Fe-containing open-framework solids. Midrow Fe was selected because it exhibits divergent behavior in both density and spin-state energetic properties for solids with both HF exchange and DFT+U. The oxidation state, spin state, and spin-specific metal−ligand bond lengths of these extracted complexes (i.e., $[Fe(OH)_6]^{4-}$, $[Fe(CO_3)_6]^{10-}$, $[Fe(NCNH)_6]^{4-}$, and $[Fe(CN)_6]^{3-}$) were kept consistent with the corresponding solids (i.e., $Fe(OH)_2$, $FeCO_3$, $Fe(NCNH)_2$, and $K_3Fe(CN)_6$) (Figure 7).



DOI: 10.1021/acs.jctc.7b01061
J. Chem. Theory Comput. 2018, 14, 670−683

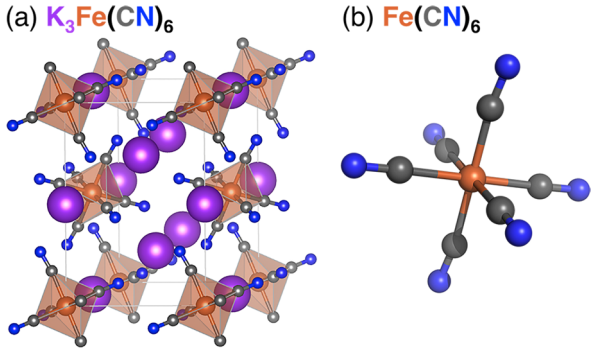


**Figure 7.** (a) Monoclinic crystal structure $K_3Fe(CN)_6$ with additional carbon and nitrogen atoms beyond the unit cell boundary to show the octahedral coordination environment of the iron atom (octahedron highlighted in translucent orange) and (b) the structure of transition-metal complex $Fe(CN)_6$ built from the corresponding crystal structure of $K_3Fe(CN)_6$. The other transition-metal complexes, $Fe(CO_3)_6$, $Fe(OH)_6$, and $Fe(NCNH)_6$, are built from their corresponding crystal structures in a similar fashion.

We first examine sensitivity of the partial charges in extracted low-spin (LS) and high-spin (HS) complexes (Figure 8).

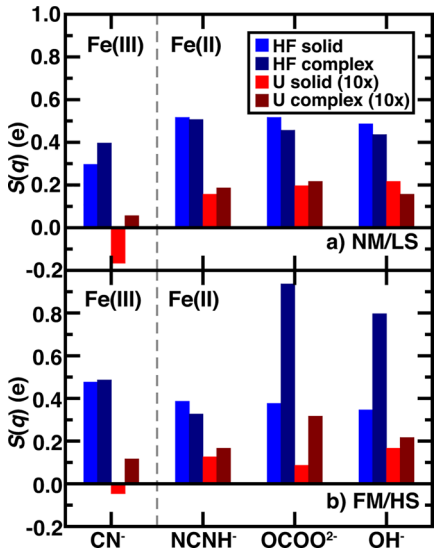


**Figure 8.** Fe partial charge sensitivities to changes in HF exchange ($e$/HFX) for solids (blue bars) and complexes (dark blue bars) and $U$ ($e$/10 eV $U$, as indicated in legend) for solids (red bars) and complexes (dark red bars) for nonmagnetic (NM) or low-spin (LS) states (top) and ferromagnetic (FM) or high-spin (HS) states (bottom) of four ligand environments. All NM/LS and FM/HS sensitivity plots span the same range: 1.2 $e$/HFX for HF exchange or 1.2 $e$/10 eV $U$ for DFT+U. The vertical dashed line distinguishes that the $CN^-$ ligand environment corresponds to Fe(III), whereas $NCNH^-$, $OCOO^{2-}$, and $OH^-$ ligand environments are Fe(II), as indicated.

Absolute values of partial charges in the extracted complexes are close to those in the solids, especially for the $MCO_3$ structures, and trends in more positive HS/FM partial charges than LS/NM partial charges are consistently preserved (Supporting Information Tables S16 and S17). The unusual partial charge sensitivities with DFT+U for solid-state $K_3Fe(CN)_6$ are absent from the $[Fe(CN)_6]^{3-}$ complex in either spin state. For the remaining ligands, the equivalent NM/LS states in solids and molecules have similar sensitivities with both methods. Although the FM/HS directions of charge localization are the same, magnitudes are generally higher in the extracted complexes for both HF exchange and DFT+U (Figure 8 and Supporting Information Table S18). Thus, these observations suggest limited transferability of the effect of functional tuning on electron density for representative clusters with respect to behavior in the solid state.

Spin-state splitting sensitivities in Fe-containing open framework solids have unexpectedly positive values in $Fe(OH)_2$ with DFT+U or $FeCO_3$ with HF exchange (Supporting Information Text S1). Computing the HS-LS spin-state splitting from single point energies on the extracted complexes can isolate the role of the crystalline environment in these effects. Extracted complexes have very close GGA spin-splittings to the equivalent solids (i.e., within ca. 5−10 kcal/mol, Supporting Information Tables S19 and S20). This equivalence is surprising, given that only some solids (e.g., $Fe(NCNH)_2$) exhibit 0.1−0.2 Å increases in the metal−ligand bond length from low-spin to high-spin that would be expected for isolated, equilibrium transition-metal complexes (Supporting Information Table S21). The positive $S_{HF}(\Delta E_{FM\text{-}NM})$ for $FeCO_3$ and $S_U(\Delta E_{FM\text{-}NM})$ for $Fe(OH)_2$ are negative for the extracted complexes (Figure 9). In all cases, HF exchange and

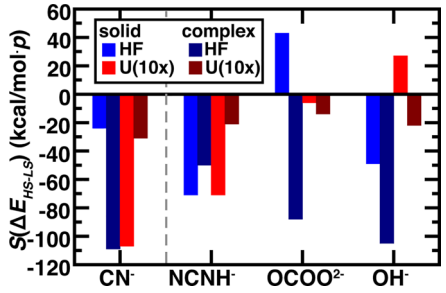


**Figure 9.** Fe magnetic or spin-state ordering sensitivity to changes in HF exchange (kcal/mol·HFX) for transition-metal solids (blue bars) and complexes (dark blue bars) and $U$ (kcal/mol·10 eV $U$, as indicated in legend) for solids (red bars) and complexes (dark red bars) of four ligand environments. The vertical dashed line distinguishes the $CN^-$ ligand environment with Fe(III), whereas $NCNH^-$, $OCOO^{2-}$, and $OH^-$ correspond to Fe(II).

DFT+U stabilize HS states of the isolated complexes, consistent with expectations from previous observations.[20−22,145] The $S_{HF}(\Delta E_{HS\text{-}LS})$ values in extracted complexes range from −108 to −49 kcal/mol·HFX, which is also consistent with typical adiabatic values in fully relaxed transition-metal complexes.[22,145] The strong ligand-field dependent effects[22,24,145] observed in DFT+U for the solids are reduced in the extracted complexes, which have little variation in $S_U(\Delta E_{HS\text{-}LS})$ (Figure 9 and Supporting Information Table S22). Thus, these observations highlight that equivalent functionals may differently affect magnetic ordering in the solid-state and spin-state ordering in transition-metal complexes.

## 4. CONCLUSIONS

We have compared the effect of two commonly employed strategies for mitigating many-electron self-interaction error within approximate DFT, i.e., DFT+U and global hybrid tuning, on the densities and magnetic ordering of a broad set of representative transition-metal-containing solids. We observed HF exchange to consistently localize density away from the metal in solids, as indicated by increasing positive partial


DOI: 10.1021/acs.jctc.7b01061
J. Chem. Theory Comput. 2018, 14, 670−683

charges, in a fashion consistent with behavior previously observed in transition-metal complexes. Conversely, DFT+U exhibited both positive (i.e., density loss at the metal) and negative (i.e., density gain at the metal) partial charge sensitivities in an electron-configuration-dependent manner. The individual metal occupation matrices and projected density of states enabled rationalization of these differing charge localization trends between HF exchange and DFT+U for early versus late transition metals. Although delocalization error in transition-metal-containing solids is often cast as a consequence of the relatively localized nature of *d* states, we confirmed that these trends in charge localization onto surrounding atoms in early transition-metal oxides for both DFT+U and HF exchange are consistently observed regardless of the surrounding coordinating atom orbital diffuseness (from 2*p* to 4*p*). Agreement of hybrids and DFT+U in early TMs and divergence on late TMs was also observed even when the metal's ligand environment was comprised of molecule-like species in open-framework solids.

We evaluated the sensitivity of magnetic-ordering to the two strategies on open-framework solids. Consistent with established trends on isolated transition-metal complexes, ferromagnetic state stabilization was observed for most transition-metal solids, albeit with single midrow exceptions each where the nonmagnetic state was instead stabilized with HF exchange ($FeCO_3$) or DFT+U ($Fe(OH)_2$). We isolated the role of the crystal environment in unexpected charge localization and magnetic state ordering by rigidly extracting complexes from the octahedral coordination environments of select open-framework solids. Our observations in the solid state of accumulation of charge density on the metal for DFT+U or stabilization of nonmagnetic states with HF exchange or DFT+U were not replicated in these isolated complexes, even though they were held fixed at the solid-state equilibrium geometries. This observation confirms the divergent behavior for DFT+U and hybrid exchange is specific to transition-metal solids. Although this work highlights the limited applicability of trends established for functional performance and the effect of tuning on transition-metal complexes even to equivalent coordination environments in the solid state, we expect this set of systems to be useful for further assessment of new delocalization error correcting methods.

## ■ ASSOCIATED CONTENT

### Supporting Information

The Supporting Information is available free of charge on the ACS Publications website at DOI: 10.1021/acs.jctc.7b01061.

Files (cif and jmol) (ZIP)

List of basis sets and pseudopotentials used; list of transition-metal solids and complexes studied; experimental and optimized lattice parameters of transition-metal solids studied; comparison of Bader charge with different resolutions of density cube file; metal partial charge sensitivities and magnetic ordering (spin-state) sensitivities of transition-metal solids (analogous complexes) and further discussion; comparison of metal partial charges between optimized and experimental lattice parameters for selected transition-metal oxides; integration of atomic orbitals in VB of PDOS; occupation matrix for "+U" correction; dependence of band gap with HF exchange for $TiO_2$ and $PtO_2$; extended discussion of magnetic ordering in open-framework solids and molecular analogues (PDF)

## ■ AUTHOR INFORMATION


### Corresponding Author

*Phone: 617-253-4584. E-mail: hjkulik@mit.edu.

### ORCID

Heather J. Kulik: 0000-0001-9342-0191



### Funding

The authors acknowledge support by the Department of Energy under grant number DE-SC0018096 and in part by the National Science Foundation under grant numbers CBET-1704266 and ECCS-1449291. H.J.K. holds a Career Award at the Scientific Interface from the Burroughs Wellcome Fund. This work was carried out in part using computational resources from the Extreme Science and Engineering Discovery Environment (XSEDE), which is supported by National Science Foundation grant number ACI-1053575.


### Notes

The authors declare no competing financial interest.

## ■ ACKNOWLEDGMENTS


The authors thank Adam H. Steeves for providing a critical reading of the manuscript.


## ■ REFERENCES


(1) Mori-Sánchez, P.; Cohen, A. J.; Yang, W. Many-Electron Self-Interaction Error in Approximate Density Functionals. *J. Chem. Phys.* **2006**, *125*, 201102.

(2) Ruzsinszky, A.; Perdew, J. P.; Csonka, G. I.; Vydrov, O. A.; Scuseria, G. E. Density Functionals That Are One- and Two- Are Not Always Many-Electron Self-Interaction-Free, as Shown for H2+, He2+, LiH+, and Ne2+. *J. Chem. Phys.* **2007**, *126*, 104102.

(3) Haunschild, R.; Henderson, T. M.; Jiménez-Hoyos, C. A.; Scuseria, G. E. Many-Electron Self-Interaction and Spin Polarization Errors in Local Hybrid Density Functionals. *J. Chem. Phys.* **2010**, *133*, 134116.

(4) Cohen, A. J.; Mori-Sánchez, P.; Yang, W. Insights into Current Limitations of Density Functional Theory. *Science* **2008**, *321*, 792–794.

(5) Schmidt, T.; Kümmel, S. One- and Many-Electron Self-Interaction Error in Local and Global Hybrid Functionals. *Phys. Rev. B: Condens. Matter Mater. Phys.* **2016**, *93*, 165120.

(6) Kim, M.-C.; Sim, E.; Burke, K. Understanding and Reducing Errors in Density Functional Calculations. *Phys. Rev. Lett.* **2013**, *111*, 073003.

(7) Zheng, X.; Liu, M.; Johnson, E. R.; Contreras-García, J.; Yang, W. Delocalization Error of Density-Functional Approximations: A Distinct Manifestation in Hydrogen Molecular Chains. *J. Chem. Phys.* **2012**, *137*, 214106.

(8) Johnson, E. R.; Otero-de-la-Roza, A.; Dale, S. G. Extreme Density-Driven Delocalization Error for a Model Solvated-Electron System. *J. Chem. Phys.* **2013**, *139*, 184116.

(9) Ruzsinszky, A.; Perdew, J. P.; Csonka, G. I.; Vydrov, O. A.; Scuseria, G. E. Spurious Fractional Charge on Dissociated Atoms: Pervasive and Resilient Self-Interaction Error of Common Density Functionals. *J. Chem. Phys.* **2006**, *125*, 194112.

(10) Dutoi, A. D.; Head-Gordon, M. Self-Interaction Error of Local Density Functionals for Alkali–Halide Dissociation. *Chem. Phys. Lett.* **2006**, *422*, 230–233.

(11) Bally, T.; Sastry, G. N. Incorrect Dissociation Behavior of Radical Ions in Density Functional Calculations. *J. Phys. Chem. A* **1997**, *101*, 7923–7925.




DOI: 10.1021/acs.jctc.7b01061
*J. Chem. Theory Comput.* 2018, 14, 670–683

(12) Zhang, Y.; Yang, W. A Challenge for Density Functionals: Self-Interaction Error Increases for Systems with a Noninteger Number of Electrons. *J. Chem. Phys.* **1998**, *109*, 2604−2608.
(13) Johnson, B. G.; Gonzales, C. A.; Gill, P. M. W.; Pople, J. A. A Density Functional Study of the Simplest Hydrogen Abstraction Reaction. Effect of Self-Interaction Correction. *Chem. Phys. Lett.* **1994**, *221*, 100−108.
(14) Mori-Sánchez, P.; Cohen, A. J.; Yang, W. Localization and Delocalization Errors in Density Functional Theory and Implications for Band-Gap Prediction. *Phys. Rev. Lett.* **2008**, *100*, 146401.
(15) Cohen, A. J.; Mori-Sánchez, P.; Yang, W. Fractional Charge Perspective on the Band Gap in Density-Functional Theory. *Phys. Rev. B: Condens. Matter Mater. Phys.* **2008**, *77*, 115123.
(16) Tozer, D. J.; De Proft, F. Computation of the Hardness and the Problem of Negative Electron Affinities in Density Functional Theory. *J. Phys. Chem. A* **2005**, *109*, 8923−8929.
(17) Teale, A. M.; De Proft, F.; Tozer, D. J. Orbital Energies and Negative Electron Affinities from Density Functional Theory: Insight from the Integer Discontinuity. *J. Chem. Phys.* **2008**, *129*, 044110.
(18) Peach, M. J. G.; Teale, A. M.; Helgaker, T.; Tozer, D. J. Fractional Electron Loss in Approximate DFT and Hartree−Fock Theory. *J. Chem. Theory Comput.* **2015**, *11*, 5262−5268.
(19) Kulik, H. J.; Cococcioni, M.; Scherlis, D. A.; Marzari, N. Density Functional Theory in Transition-Metal Chemistry: A Self-Consistent Hubbard U Approach. *Phys. Rev. Lett.* **2006**, *97*, 103001.
(20) Ganzenmüller, G.; Berkaïne, N.; Fouqueau, A.; Casida, M. E.; Reiher, M. Comparison of Density Functionals for Differences between the High-(T 2 G 5) and Low-(a 1 G 1) Spin States of Iron (II) Compounds. IV. Results for the Ferrous Complexes [Fe (L)('Nhs 4')]. *J. Chem. Phys.* **2005**, *122*, 234321.
(21) Droghetti, A.; Alfè, D.; Sanvito, S. Assessment of Density Functional Theory for Iron (II) Molecules across the Spin-Crossover Transition. *J. Chem. Phys.* **2012**, *137*, 124303.
(22) Ioannidis, E. I.; Kulik, H. J. Towards Quantifying the Role of Exact Exchange in Predictions of Transition Metal Complex Properties. *J. Chem. Phys.* **2015**, *143*, 034104.
(23) Mortensen, S. R.; Kepp, K. P. Spin Propensities of Octahedral Complexes from Density Functional Theory. *J. Phys. Chem. A* **2015**, *119*, 4041−4050.
(24) Ioannidis, E. I.; Kulik, H. J. Ligand-Field-Dependent Behavior of Meta-GGA Exchange in Transition-Metal Complex Spin-State Ordering. *J. Phys. Chem. A* **2017**, *121*, 874−884.
(25) Da Silva, J. L.; Ganduglia-Pirovano, M. V.; Sauer, J.; Bayer, V.; Kresse, G. Hybrid Functionals Applied to Rare-Earth Oxides: The Example of Ceria. *Phys. Rev. B: Condens. Matter Mater. Phys.* **2007**, *75*, 045121.
(26) Ping, Y.; Galli, G.; Goddard, W. A., III Electronic Structure of Iro2: The Role of the Metal d Orbitals. *J. Phys. Chem. C* **2015**, *119*, 11570−11577.
(27) He, J.; Chen, M.-X.; Chen, X.-Q.; Franchini, C. Structural Transitions and Transport-Half-Metallic Ferromagnetism in Lamno 3 at Elevated Pressure. *Phys. Rev. B: Condens. Matter Mater. Phys.* **2012**, *85*, 195135.
(28) Perdew, J. P.; Parr, R. G.; Levy, M.; Balduz, J. L. Density-Functional Theory for Fractional Particle Number: Derivative Discontinuities of the Energy. *Phys. Rev. Lett.* **1982**, *49*, 1691−1694.
(29) Perdew, J. P.; Levy, M. Physical Content of the Exact Kohn-Sham Orbital Energies: Band Gaps and Derivative Discontinuities. *Phys. Rev. Lett.* **1983**, *51*, 1884−1887.
(30) Sham, L. J.; Schlüter, M. Density-Functional Theory of the Energy Gap. *Phys. Rev. Lett.* **1983**, *51*, 1888−1891.
(31) Sagvolden, E.; Perdew, J. P. Discontinuity of the Exchange-Correlation Potential: Support for Assumptions Used to Find It. *Phys. Rev. A: At., Mol., Opt. Phys.* **2008**, *77*, 012517.
(32) Mori-Sanchez, P.; Cohen, A. J. The Derivative Discontinuity of the Exchange-Correlation Functional. *Phys. Chem. Chem. Phys.* **2014**, *16*, 14378−14387.
(33) Vydrov, O. A.; Scuseria, G. E.; Perdew, J. P. Tests of Functionals for Systems with Fractional Electron Number. *J. Chem. Phys.* **2007**, *126*, 154109.
(34) Yang, W.; Zhang, Y.; Ayers, P. W. Degenerate Ground States and a Fractional Number of Electrons in Density and Reduced Density Matrix Functional Theory. *Phys. Rev. Lett.* **2000**, *84*, 5172−5175.
(35) Leininger, T.; Stoll, H.; Werner, H.-J.; Savin, A. Combining Long-Range Configuration Interaction with Short-Range Density Functionals. *Chem. Phys. Lett.* **1997**, *275*, 151−160.
(36) Toulouse, J.; Colonna, F.; Savin, A. Long-Range-Short-Range Separation of the Electron-Electron Interaction in Density-Functional Theory. *Phys. Rev. A: At., Mol., Opt. Phys.* **2004**, *70*, 062505.
(37) Vydrov, O. A.; Scuseria, G. E. Assessment of a Long-Range Corrected Hybrid Functional. *J. Chem. Phys.* **2006**, *125*, 234109.
(38) Cohen, A. J.; Mori-Sánchez, P.; Yang, W. Development of Exchange-Correlation Functionals with Minimal Many-Electron Self-Interaction Error. *J. Chem. Phys.* **2007**, *126*, 191109.
(39) Iikura, H.; Tsuneda, T.; Yanai, T.; Hirao, K. A Long-Range Correction Scheme for Generalized-Gradient-Approximation Exchange Functionals. *J. Chem. Phys.* **2001**, *115*, 3540−3544.
(40) Baer, R.; Neuhauser, D. Density Functional Theory with Correct Long-Range Asymptotic Behavior. *Phys. Rev. Lett.* **2005**, *94*, 043002.
(41) Tsuneda, T.; Song, J.-W.; Suzuki, S.; Hirao, K. On Koopmans' Theorem in Density Functional Theory. *J. Chem. Phys.* **2010**, *133*, 174101.
(42) Livshits, E.; Baer, R. A Well-Tempered Density Functional Theory of Electrons in Molecules. *Phys. Chem. Chem. Phys.* **2007**, *9*, 2932−2941.
(43) Kronik, L.; Stein, T.; Refaely-Abramson, S.; Baer, R. Excitation Gaps of Finite-Sized Systems from Optimally Tuned Range-Separated Hybrid Functionals. *J. Chem. Theory Comput.* **2012**, *8*, 1515−1531.
(44) Stein, T.; Kronik, L.; Baer, R. Reliable Prediction of Charge Transfer Excitations in Molecular Complexes Using Time-Dependent Density Functional Theory. *J. Am. Chem. Soc.* **2009**, *131*, 2818−2820.
(45) Stein, T.; Kronik, L.; Baer, R. Prediction of Charge-Transfer Excitations in Coumarin-Based Dyes Using a Range-Separated Functional Tuned from First Principles. *J. Chem. Phys.* **2009**, *131*, 244119.
(46) Srebro, M.; Autschbach, J. Does a Molecule-Specific Density Functional Give an Accurate Electron Density? The Challenging Case of the Cucl Electric Field Gradient. *J. Phys. Chem. Lett.* **2012**, *3*, 576−581.
(47) Körzdörfer, T.; Brédas, J.-L. Organic Electronic Materials: Recent Advances in the DFT Description of the Ground and Excited States Using Tuned Range-Separated Hybrid Functionals. *Acc. Chem. Res.* **2014**, *47*, 3284−3291.
(48) Autschbach, J.; Srebro, M. Delocalization Error and "Functional Tuning" in Kohn−Sham Calculations of Molecular Properties. *Acc. Chem. Res.* **2014**, *47*, 2592−2602.
(49) Gledhill, J. D.; Peach, M. J. G.; Tozer, D. J. Assessment of Tuning Methods for Enforcing Approximate Energy Linearity in Range-Separated Hybrid Functionals. *J. Chem. Theory Comput.* **2013**, *9*, 4414−4420.
(50) Stein, T.; Eisenberg, H.; Kronik, L.; Baer, R. Fundamental Gaps in Finite Systems from Eigenvalues of a Generalized Kohn-Sham Method. *Phys. Rev. Lett.* **2010**, *105*, 266802.
(51) Salzner, U.; Baer, R. Koopmans' Springs to Life. *J. Chem. Phys.* **2009**, *131*, 231101.
(52) Janak, J. F. Proof That dE/dni = Epsilon in Density-Functional Theory. *Phys. Rev. B: Condens. Matter Mater. Phys.* **1978**, *18*, 7165−7168.
(53) Stein, T.; Autschbach, J.; Govind, N.; Kronik, L.; Baer, R. Curvature and Frontier Orbital Energies in Density Functional Theory. *J. Phys. Chem. Lett.* **2012**, *3*, 3740−3744.
(54) Körzdörfer, T.; Sears, J. S.; Sutton, C.; Brédas, J.-L. Long-Range Corrected Hybrid Functionals for π-Conjugated Systems: Dependence of the Range-Separation Parameter on Conjugation Length. *J. Chem. Phys.* **2011**, *135*, 204107.


DOI: 10.1021/acs.jctc.7b01061
*J. Chem. Theory Comput.* 2018, 14, 670−683

(55) Karolewski, A.; Kronik, L.; Kümmel, S. Using Optimally Tuned Range Separated Hybrid Functionals in Ground-State Calculations: Consequences and Caveats. *J. Chem. Phys.* **2013**, *138*, 204115.
(56) Whittleton, S. R.; Sosa Vazquez, X. A.; Isborn, C. M.; Johnson, E. R. Density-Functional Errors in Ionization Potential with Increasing System Size. *J. Chem. Phys.* **2015**, *142*, 184106.
(57) Vlček, V.; Eisenberg, H. R.; Steinle-Neumann, G.; Kronik, L.; Baer, R. Deviations from Piecewise Linearity in the Solid-State Limit with Approximate Density Functionals. *J. Chem. Phys.* **2015**, *142*, 034107.
(58) Zhao, Q.; Ioannidis, E. I.; Kulik, H. J. Global and Local Curvature in Density Functional Theory. *J. Chem. Phys.* **2016**, *145*, 054109.
(59) Anisimov, V. I.; Zaanen, J.; Andersen, O. K. Band Theory and Mott Insulators - Hubbard-U Instead of Stoner-I. *Phys. Rev. B: Condens. Matter Mater. Phys.* **1991**, *44*, 943−954.
(60) Liechtenstein, A. I.; Anisimov, V. I.; Zaanen, J. Density-Functional Theory and Strong-Interactions - Orbital Ordering in Mott-Hubbard Insulators. *Phys. Rev. B: Condens. Matter Mater. Phys.* **1995**, *52*, R5467−R5470.
(61) Kulik, H. J. Perspective: Treating Electron Over-delocalization with the DFT+ U Method. *J. Chem. Phys.* **2015**, *142*, 240901.
(62) Pickett, W. E.; Erwin, S. C.; Ethridge, E. C. Reformulation of the LDA+U Method for a Local-Orbital Basis. *Phys. Rev. B: Condens. Matter Mater. Phys.* **1998**, *58*, 1201−1209.
(63) Cococcioni, M.; De Gironcoli, S. Linear Response Approach to the Calculation of the Effective Interaction Parameters in the LDA+ U Method. *Phys. Rev. B: Condens. Matter Mater. Phys.* **2005**, *71*, 035105.
(64) Lee, C.; Yang, W.; Parr, R. G. Development of the Colle-Salvetti Correlation-Energy Formula into a Functional of the Electron Density. *Phys. Rev. B: Condens. Matter Mater. Phys.* **1988**, *37*, 785−789.
(65) Becke, A. D. Density-Functional Thermochemistry. III. The Role of Exact Exchange. *J. Chem. Phys.* **1993**, *98*, 5648−5652.
(66) Stephens, P. J.; Devlin, F. J.; Chabalowski, C. F.; Frisch, M. J. Ab Initio Calculation of Vibrational Absorption and Circular Dichroism Spectra Using Density Functional Force Fields. *J. Phys. Chem.* **1994**, *98*, 11623−11627.
(67) Bochevarov, A. D.; Friesner, R. A. The Densities Produced by the Density Functional Theory: Comparison to Full Configuration Interaction. *J. Chem. Phys.* **2008**, *128*, 034102.
(68) He, Y.; Gräfenstein, J.; Kraka, E.; Cremer, D. What Correlation Effects Are Covered by Density Functional Theory? *Mol. Phys.* **2000**, *98*, 1639−1658.
(69) Bader, R. F. W. A Quantum Theory of Molecular Structure and Its Applications. *Chem. Rev.* **1991**, *91*, 893−928.
(70) Kepp, K. P. Comment on "Density Functional Theory Is Straying from the Path toward the Exact Functional. *Science* **2017**, *356*, 496.2.
(71) Medvedev, M. G.; Bushmarinov, I. S.; Sun, J.; Perdew, J. P.; Lyssenko, K. A. Density Functional Theory Is Straying from the Path toward the Exact Functional. *Science* **2017**, *355*, 49−52.
(72) Brorsen, K. R.; Yang, Y.; Pak, M. V.; Hammes-Schiffer, S. Is the Accuracy of Density Functional Theory for Atomization Energies and Densities in Bonding Regions Correlated? *J. Phys. Chem. Lett.* **2017**, *8*, 2076−2081.
(73) Mezei, P. D.; Csonka, G. I.; Kállay, M. Electron Density Errors and Density-Driven Exchange-Correlation Energy Errors in Approximate Density Functional Calculations. *J. Chem. Theory Comput.* **2017**, *13*, 4753−4764.
(74) Gani, T. Z.; Kulik, H. J. Where Does the Density Localize? Convergent Behavior for Global Hybrids, Range Separation, and DFT + U. *J. Chem. Theory Comput.* **2016**, *12*, 5931−5945.
(75) Brumboiu, I. E.; Prokopiou, G.; Kronik, L.; Brena, B. Valence Electronic Structure of Cobalt Phthalocyanine from an Optimally Tuned Range-Separated Hybrid Functional. *J. Chem. Phys.* **2017**, *147*, 044301.
(76) Duignan, T. J.; Autschbach, J. Impact of the Kohn−Sham Delocalization Error on the 4f Shell Localization and Population in Lanthanide Complexes. *J. Chem. Theory Comput.* **2016**, *12*, 3109−3121.
(77) Duignan, T. J.; Autschbach, J.; Batista, E.; Yang, P. Assessment of Tuned Range Separated Exchange Functionals for Spectroscopies and Properties of Uranium Complexes. *J. Chem. Theory Comput.* **2017**, *13*, 3614−3625.
(78) Pritchard, B.; Autschbach, J. Theoretical Investigation of Paramagnetic NMR Shifts in Transition Metal Acetylacetonato Complexes: Analysis of Signs, Magnitudes, and the Role of the Covalency of Ligand−Metal Bonding. *Inorg. Chem.* **2012**, *51*, 8340−8351.
(79) Janesko, B. G.; Scuseria, G. E. Hartree−Fock Orbitals Significantly Improve the Reaction Barrier Heights Predicted by Semilocal Density Functionals. *J. Chem. Phys.* **2008**, *128*, 244112.
(80) Verma, P.; Perera, A.; Bartlett, R. J. Increasing the Applicability of DFT I: Non-Variational Correlation Corrections from Hartree−Fock DFT for Predicting Transition States. *Chem. Phys. Lett.* **2012**, *524*, 10−15.
(81) Kim, M.-C.; Sim, E.; Burke, K. Ions in Solution: Density Corrected Density Functional Theory (DC-DFT). *J. Chem. Phys.* **2014**, *140*, 18A528.
(82) Kim, M.-C.; Park, H.; Son, S.; Sim, E.; Burke, K. Improved DFT Potential Energy Surfaces via Improved Densities. *J. Phys. Chem. Lett.* **2015**, *6*, 3802−3807.
(83) Hubbard, J. Electron Correlations in Narrow Energy Bands. *Proc. R. Soc. London, Ser. A* **1963**, *276*, 238−257.
(84) Anderson, P. W. Localized Magnetic States in Metals. *Phys. Rev.* **1961**, *124*, 41−53.
(85) Janet, J. P.; Zhao, Q.; Ioannidis, E. I.; Kulik, H. J. Density Functional Theory for Modeling Large Molecular Adsorbate-Surface Interactions: A Mini-Review and Worked Example. *Mol. Simul.* **2017**, *43*, 327−345.
(86) Gani, T. Z. H.; Kulik, H. J. Unifying Exchange Sensitivity in Transition Metal Spin-State Ordering and Catalysis through Bond Valence Metrics. *J. Chem. Theory Comput.* **2017**, *13*, 5443.
(87) Verma, P.; Truhlar, D. G. Does DFT+ U Mimic Hybrid Density Functionals? *Theor. Chem. Acc.* **2016**, *135*, 1−15.
(88) Loschen, C.; Carrasco, J.; Neyman, K. M.; Illas, F. First-Principles LDA+ U and GGA+ U Study of Cerium Oxides: Dependence on the Effective U Parameter. *Phys. Rev. B: Condens. Matter Mater. Phys.* **2007**, *75*, 035115.
(89) Andersson, D. A.; Simak, S.; Johansson, B.; Abrikosov, I.; Skorodumova, N. V. Modeling of Ce O 2, Ce 2 O 3, and Ce O 2− X in the LDA+ U Formalism. *Phys. Rev. B: Condens. Matter Mater. Phys.* **2007**, *75*, 035109.
(90) Shao, G. Red Shift in Manganese-and Iron-Doped Tio2: A DFT + U Analysis. *J. Phys. Chem. C* **2009**, *113*, 6800−6808.
(91) Hu, Z.; Metiu, H. Choice of U for DFT+ U Calculations for Titanium Oxides. *J. Phys. Chem. C* **2011**, *115*, 5841−5845.
(92) Rödl, C.; Fuchs, F.; Furthmüller, J.; Bechstedt, F. Quasiparticle Band Structures of the Antiferromagnetic Transition-Metal Oxides MnO, FeO, CoO, and NiO. *Phys. Rev. B: Condens. Matter Mater. Phys.* **2009**, *79*, 235114.
(93) Tran, F.; Blaha, P.; Schwarz, K.; Novák, P. Hybrid Exchange-Correlation Energy Functionals for Strongly Correlated Electrons: Applications to Transition-Metal Monoxides. *Phys. Rev. B: Condens. Matter Mater. Phys.* **2006**, *74*, 155108.
(94) Franchini, C.; Podloucky, R.; Paier, J.; Marsman, M.; Kresse, G. Ground-State Properties of Multivalent Manganese Oxides: Density Functional and Hybrid Density Functional Calculations. *Phys. Rev. B: Condens. Matter Mater. Phys.* **2007**, *75*, 195128.
(95) Liao, P.; Carter, E. A. Testing Variations of the Gw Approximation on Strongly Correlated Transition Metal Oxides: Hematite (A-Fe 2 O 3) as a Benchmark. *Phys. Chem. Chem. Phys.* **2011**, *13*, 15189−15199.
(96) Rollmann, G.; Rohrbach, A.; Entel, P.; Hafner, J. First-Principles Calculation of the Structure and Magnetic Phases of Hematite. *Phys. Rev. B: Condens. Matter Mater. Phys.* **2004**, *69*, 165107.


DOI: 10.1021/acs.jctc.7b01061
*J. Chem. Theory Comput.* 2018, 14, 670−683

(97) Hong, J.; Stroppa, A.; Íñiguez, J.; Picozzi, S.; Vanderbilt, D. Spin-Phonon Coupling Effects in Transition-Metal Perovskites: A DFT+ U and Hybrid-Functional Study. *Phys. Rev. B: Condens. Matter Mater. Phys.* **2012**, *85*, 054417.
(98) Seo, D.-H.; Urban, A.; Ceder, G. Calibrating Transition-Metal Energy Levels and Oxygen Bands in First-Principles Calculations: Accurate Prediction of Redox Potentials and Charge Transfer in Lithium Transition-Metal Oxides. *Phys. Rev. B: Condens. Matter Mater. Phys.* **2015**, *92*, 115118.
(99) Franchini, C.; Bayer, V.; Podloucky, R.; Paier, J.; Kresse, G. Density Functional Theory Study of MnO by a Hybrid Functional Approach. *Phys. Rev. B: Condens. Matter Mater. Phys.* **2005**, *72*, 045132.
(100) Gerosa, M.; Bottani, C. E.; Caramella, L.; Onida, G.; Di Valentin, C.; Pacchioni, G. Electronic Structure and Phase Stability of Oxide Semiconductors: Performance of Dielectric-Dependent Hybrid Functional DFT, Benchmarked against G W Band Structure Calculations and Experiments. *Phys. Rev. B: Condens. Matter Mater. Phys.* **2015**, *91*, 155201.
(101) Graciani, J.; Márquez, A. M.; Plata, J. J.; Ortega, Y.; Hernández, N. C.; Meyer, A.; Zicovich-Wilson, C. M.; Sanz, J. F. Comparative Study on the Performance of Hybrid DFT Functionals in Highly Correlated Oxides: The Case of Ceo2 and Ce2o3. *J. Chem. Theory Comput.* **2011**, *7*, 56−65.
(102) Pozun, Z. D.; Henkelman, G. Hybrid Density Functional Theory Band Structure Engineering in Hematite. *J. Chem. Phys.* **2011**, *134*, 224706.
(103) He, J.; Franchini, C. Screened Hybrid Functional Applied to 3 d 0→ 3 d 8 Transition-Metal Perovskites La M O 3 (M= Sc−Cu): Influence of the Exchange Mixing Parameter on the Structural, Electronic, and Magnetic Properties. *Phys. Rev. B: Condens. Matter Mater. Phys.* **2012**, *86*, 235117.
(104) Viñes, F.; Lamiel-García, O.; Chul Ko, K.; Yong Lee, J.; Illas, F. Systematic Study of the Effect of HSE Functional Internal Parameters on the Electronic Structure and Band Gap of a Representative Set of Metal Oxides. *J. Comput. Chem.* **2017**, *38*, 781−789.
(105) Guo, Y.; Clark, S. J.; Robertson, J. Electronic and Magnetic Properties of Ti2o3, Cr2o3, and Fe2o3 Calculated by the Screened Exchange Hybrid Density Functional. *J. Phys.: Condens. Matter* **2012**, *24*, 325504.
(106) Dovesi, R.; Orlando, R.; Erba, A.; Zicovich-Wilson, C. M.; Civalleri, B.; Casassa, S.; Maschio, L.; Ferrabone, M.; De La Pierre, M.; D'Arco, P. Crystal14: A Program for the Ab Initio Investigation of Crystalline Solids. *Int. J. Quantum Chem.* **2014**, *114*, 1287−1317.
(107) Vosko, S. H.; Wilk, L.; Nusair, M. Accurate Spin-Dependent Electron Liquid Correlation Energies for Local Spin Density Calculations: A Critical Analysis. *Can. J. Phys.* **1980**, *58*, 1200−1211.
(108) CRYSTAL. http://www.crystal.unito.it/ (accessed October 11, 2017).
(109) Wadt, W. R.; Hay, P. J. Ab Initio Effective Core Potentials for Molecular Calculations. Potentials for Main Group Elements Na to Bi. *J. Chem. Phys.* **1985**, *82*, 284−298.
(110) Broyden, C. G. The Convergence of a Class of Double-Rank Minimization Algorithms 1. General Considerations. *IMA J. Appl. Math.* **1970**, *6*, 76−90.
(111) Broyden, C. G. The Convergence of a Class of Double-Rank Minimization Algorithms: 2. The New Algorithm. *IMA J. Appl. Math.* **1970**, *6*, 222−231.
(112) Fletcher, R. A New Approach to Variable Metric Algorithms. *Comput. J.* **1970**, *13*, 317−322.
(113) Goldfarb, D. A Family of Variable-Metric Methods Derived by Variational Means. *Math. Comput.* **1970**, *24*, 23−26.
(114) Shanno, D. F. Conditioning of Quasi-Newton Methods for Function Minimization. *Math. Comput.* **1970**, *24*, 647−656.
(115) Petachem. http://www.petachem.com (accessed October 11, 2017).
(116) Ufimtsev, I. S.; Martinez, T. J. Quantum Chemistry on Graphical Processing Units. 3. Analytical Energy Gradients, Geometry Optimization, and First Principles Molecular Dynamics. *J. Chem. Theory Comput.* **2009**, *5*, 2619−2628.
(117) Hay, P. J.; Wadt, W. R. Ab Initio Effective Core Potentials for Molecular Calculations. Potentials for the Transition Metal Atoms Sc to Hg. *J. Chem. Phys.* **1985**, *82*, 270−283.
(118) Saunders, V.; Hillier, I. A "Level−Shifting" Method for Converging Closed Shell Hartree−Fock Wave Functions. *Int. J. Quantum Chem.* **1973**, *7*, 699−705.
(119) Dudarev, S. L.; Botton, G. A.; Savrasov, S. Y.; Humphreys, C. J.; Sutton, A. P. Electron-Energy-Loss Spectra and the Structural Stability of Nickel Oxide: An LSDA+U Study. *Phys. Rev. B: Condens. Matter Mater. Phys.* **1998**, *57*, 1505−1509.
(120) Giannozzi, P.; Baroni, S.; Bonini, N.; Calandra, M.; Car, R.; Cavazzoni, C.; Ceresoli, D.; Chiarotti, G. L.; Cococcioni, M.; Dabo, I. Quantum Espresso: A Modular and Open-Source Software Project for Quantum Simulations of Materials. *J. Phys.: Condens. Matter* **2009**, *21*, 395502.
(121) Perdew, J. P.; Burke, K.; Ernzerhof, M. Generalized Gradient Approximation Made Simple. *Phys. Rev. Lett.* **1996**, *77*, 3865.
(122) Vanderbilt, D. Soft Self-Consistent Pseudopotentials in a Generalized Eigenvalue Formalism. *Phys. Rev. B: Condens. Matter Mater. Phys.* **1990**, *41*, 7892.
(123) Quantum-Espresso. http://www.quantum-espresso.org/ (accessed October 11, 2017).
(124) Martyna, G. J.; Tuckerman, M. E. A Reciprocal Space Based Method for Treating Long Range Interactions in Ab Initio and Force-Field-Based Calculations in Clusters. *J. Chem. Phys.* **1999**, *110*, 2810−2821.
(125) Kulik, H. J.; Marzari, N. A Self-Consistent Hubbard U Density-Functional Theory Approach to the Addition-Elimination Reactions of Hydrocarbons on Bare FeO+. *J. Chem. Phys.* **2008**, *129*, 134314.
(126) Hellenbrandt, M. The Inorganic Crystal Structure Database (ICSD)—Present and Future. *Crystallogr. Rev.* **2004**, *10*, 17−22.
(127) Hanwell, M. D.; Curtis, D. E.; Lonie, D. C.; Vandermeersch, T.; Zurek, E.; Hutchison, G. R. Avogadro: An Advanced Semantic Chemical Editor, Visualization, and Analysis Platform. *J. Cheminf.* **2012**, *4*, 17.
(128) Bader, R. F. *Atoms in Molecules*; Wiley Online Library: 1990; DOI: 10.1002/0470845015.caa012
(129) Tang, W.; Sanville, E.; Henkelman, G. A Grid-Based Bader Analysis Algorithm without Lattice Bias. *J. Phys.: Condens. Matter* **2009**, *21*, 084204.
(130) Lu, T.; Chen, F. Multiwfn: A Multifunctional Wavefunction Analyzer. *J. Comput. Chem.* **2012**, *33*, 580−592.
(131) Deskins, N. A.; Dupuis, M. Electron Transport via Polaron Hopping in Bulk Ti O 2: A Density Functional Theory Characterization. *Phys. Rev. B: Condens. Matter Mater. Phys.* **2007**, *75*, 195212.
(132) Martinez, J. I.; Hansen, H. A.; Rossmeisl, J.; Nørskov, J. K. Formation Energies of Rutile Metal Dioxides Using Density Functional Theory. *Phys. Rev. B: Condens. Matter Mater. Phys.* **2009**, *79*, 045120.
(133) Morgan, B. J.; Watson, G. W. A Density Functional Theory+ U Study of Oxygen Vacancy Formation at the (110),(100),(101), and (001) Surfaces of Rutile Tio2. *J. Phys. Chem. C* **2009**, *113*, 7322−7328.
(134) Umebayashi, T.; Yamaki, T.; Itoh, H.; Asai, K. Analysis of Electronic Structures of 3d Transition Metal-Doped Tio 2 Based on Band Calculations. *J. Phys. Chem. Solids* **2002**, *63*, 1909−1920.
(135) Wang, L.; Maxisch, T.; Ceder, G. Oxidation Energies of Transition Metal Oxides within the GGA+ U Framework. *Phys. Rev. B: Condens. Matter Mater. Phys.* **2006**, *73*, 195107.
(136) Muscat, J.; Wander, A.; Harrison, N. On the Prediction of Band Gaps from Hybrid Functional Theory. *Chem. Phys. Lett.* **2001**, *342*, 397−401.
(137) Pascual, J.; Camassel, J.; Mathieu, H. Fine Structure in the Intrinsic Absorption Edge of Ti O 2. *Phys. Rev. B: Condens. Matter Mater. Phys.* **1978**, *18*, 5606.
(138) Amtout, A.; Leonelli, R. Optical Properties of Rutile near Its Fundamental Band Gap. *Phys. Rev. B: Condens. Matter Mater. Phys.* **1995**, *51*, 6842.


DOI: 10.1021/acs.jctc.7b01061
*J. Chem. Theory Comput.* 2018, 14, 670−683

(139) Strehlow, W.; Cook, E. Compilation of Energy Band Gaps in Elemental and Binary Compound Semiconductors and Insulators. *J. Phys. Chem. Ref. Data* **1973**, *2*, 163−200.
(140) Zheng, X.; Cohen, A. J.; Mori-Sánchez, P.; Hu, X.; Yang, W. Improving Band Gap Prediction in Density Functional Theory from Molecules to Solids. *Phys. Rev. Lett.* **2011**, *107*, 026403.
(141) Zhou, F.; Kang, K.; Maxisch, T.; Ceder, G.; Morgan, D. The Electronic Structure and Band Gap of Lifepo 4 and Limnpo 4. *Solid State Commun.* **2004**, *132*, 181−186.
(142) Marques, M. A.; Vidal, J.; Oliveira, M. J.; Reining, L.; Botti, S. Density-Based Mixing Parameter for Hybrid Functionals. *Phys. Rev. B: Condens. Matter Mater. Phys.* **2011**, *83*, 035119.
(143) Wemple, S. Optical Oscillator Strengths and Excitation Energies in Solids, Liquids, and Molecules. *J. Chem. Phys.* **1977**, *67*, 2151−2168.
(144) Kulik, H. J.; Marzari, N. Systematic Study of First-Row Transition-Metal Diatomic Molecules: A Self-Consistent DFT Plus U Approach. *J. Chem. Phys.* **2010**, *133*, 114103.
(145) Janet, J. P.; Kulik, H. J. Predicting Electronic Structure Properties of Transition Metal Complexes with Neural Networks. *Chem. Sci.* **2017**, *8*, 5137−5152.



DOI: 10.1021/acs.jctc.7b01061
*J. Chem. Theory Comput.* 2018, 14, 670−683